

Spatial harmonic distortion: a test for focal plane nonlinearity

Glenn D. Boreman, MEMBER SPIE

Anthony B. James

University of Central Florida
Electrical Engineering Department
Center for Research in Electro-Optics and
Lasers
Orlando, Florida 32816

Christopher R. Costanzo, MEMBER SPIE

U.S. Army Night Vision and Electro-
Optics Center
Infrared Technology Division
Ft. Belvoir, Virginia 22060

Abstract. A new measurement technique for focal plane linearity was investigated experimentally. The spatial harmonic distortion test consists of projecting spatial sine waves of irradiance onto a focal plane by means of a Young's fringe technique. If the detectors in the array have a linear responsivity, a sinusoidal input waveform is mapped to a sinusoidal output. However, if the detectors in the array have a nonlinear responsivity (i.e., saturation), then the output waveform will exhibit harmonic distortion. When the Fourier transform of the array data is taken, the content at the second and third harmonics of the original sine-wave spatial frequency indicates the amount of nonlinearity in the aggregate array response. Measurement results are included for two focal planes: a vidicon tube camera and a solid-state charge-injection device (CID) camera. The minimum harmonic distortion measured was 3%. The sensitivity of this test is limited ultimately by the amount of spatial nonuniformity. Numerical and analytical models are given that indicate the minimum detectable harmonic distortion is in the range of a few percent. This test also allows measurement of the spatial-frequency dependence of the nonlinearity, a quantity that is not accessible with the usual flat-field techniques for linearity assessment.

Subject terms: focal planes; detector arrays; charge-coupled devices; charge-transfer devices; nonlinearity; nonuniformity; harmonic distortion; flat-field test.

Optical Engineering 30(5), 609-614 (May 1991).

CONTENTS

1. Introduction
2. Experimental setup
3. Data processing
4. Results
 - 4.1. Flat-field plots
 - 4.2. Direct waveforms
 - 4.3. Responsivity curves
 - 4.4. Spectra
 - 4.5. Percent harmonic distortion versus spatial frequency
5. Test sensitivity limitation: spatial nonuniformity
 - 5.1. Numerical model
 - 5.2. Analytical model
6. Conclusions
7. Acknowledgment
8. References

1. INTRODUCTION

A new method was investigated for the characterization of nonlinearity in detector arrays. The usual technique for linearity characterization, the flat-field method,¹⁻³ requires that the response of the array be measured for a number of uniform irradiance inputs. A responsivity (output per unit input) function then can be plotted for individual detectors or for an average detector of the array.

Distortion of waveforms by a nonlinear transfer characteristic is a well-known effect in time-domain systems.⁴ Departures from linearity of the input-output curve cause harmonic distortion in the output waveforms. The method described in this paper uses a spatial-domain analog of this process. Our technique, the spatial-harmonic-distortion test, measures the response of the array to a spatial sine wave of irradiance. These fringes are produced by Young's double-slit interference. If the detectors in the array have a linear responsivity, then the output waveform is undistorted. However, if the detectors in the array have a nonlinear response characteristic, then the output waveform exhibits harmonic distortion. The Fourier transform of the array data reveals any content at the second and third harmonics of the original sine-wave spatial frequency, proportional to the amount of nonlinearity present in the array response.

Experimental results are presented for two representative visible focal planes: a vidicon tube and a solid-state charge-injection-device (CID) array. Depending on only double-slit interference, the spatial-harmonic-distortion method is equally well suited for measuring linearity in infrared focal planes.

Our technique has a number of advantages over the usual flat-field method for linearity measurement. Since the amplitude of the input sine wave may be adjusted to cover any given range of irradiance, the entire operating characteristic of the array (at one spatial frequency) is available from a single frame of data. Also, the percent harmonic distortion is a convenient summary measure of the amount of nonlinearity of the entire focal plane.

The presence of harmonic content in the output waveform is a sensitive characterization, yielding measurable amounts of

Paper 2733 received May 5, 1989; revised manuscript received Nov. 16, 1990; accepted for publication Nov. 18, 1990.

© 1991 Society of Photo-Optical Instrumentation Engineers.

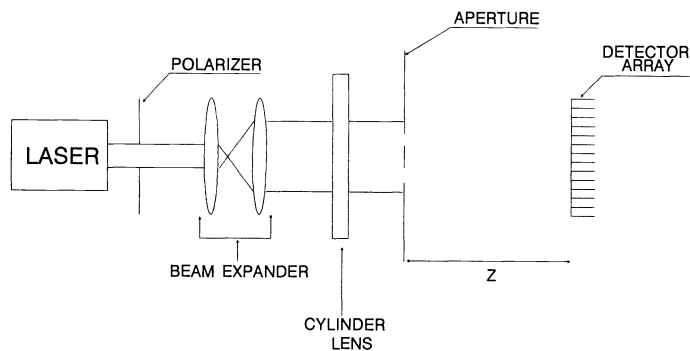


Fig. 1. Schematic of Young's fringe apparatus.

nonlinearity even for focal planes that are very linear. Thus this technique might be appropriate for a production-level linearity test of focal planes such as monolithic PtSi.

Finally, our method allows measurement of the spatial-frequency dependence of the nonlinearity. This information is not available from a flat-field test, which is a zero-spatial-frequency measurement. The dependence of nonlinearity on spatial frequency is a generalization of the linearity concept and is an effect in detector arrays somewhat analogous to the adjacency effects⁵ seen in photographic media.

2. EXPERIMENTAL SETUP

Figure 1 is a schematic of Young's double-slit apparatus that projected sinusoidal fringes onto the focal planes. The laser used was a He-Ne, with $\lambda = 0.6328 \mu\text{m}$. A cylindrical lens illuminated the pinholes, thus avoiding unnecessary dilution of irradiance in the aperture. The polarizer controlled the maximum irradiance level of the diffraction pattern. The aperture used was two square pinholes, each of dimensions $12 \mu\text{m} \times 12 \mu\text{m}$, separated by a distance of $950 \mu\text{m}$.

The diffraction pattern from this aperture has an irradiance envelope function $W(x)$ caused by the finite size of the pinholes⁶

$$W(x) = \left[\frac{\sin\left(\frac{\pi ax}{z\lambda}\right)}{\frac{\pi ax}{z\lambda}} \right]^2, \quad (1)$$

where a is the pinhole width and x is the position in the receiver plane, measured from the axis. The maximum value of x was 4 mm for the arrays tested. The aperture-to-focal-plane distance z was varied between 40 and 110 cm to produce spatial frequencies between 40 and 12.5 cycles/cm at the array plane. Given detector spacings on the focal planes of $25 \mu\text{m}$, these waveforms were oversampled, with at least 10 samples per cycle.

With the apparatus configured ($z = 40$ cm) to produce the maximum spatial frequency, Eq. (1) yields $W(x) = 0.88$ at the edges of the detector. Because the fringe data are interpreted in the Fourier domain, a nonunity $W(x)$ will broaden peaks in the spectra corresponding to harmonic content,⁷ but will not change the relative strength of these components. For lower spatial frequencies (larger z values) $W(x)$ is essentially unity over the array dimensions.

3. DATA PROCESSING

After the array data for any specific spatial frequency are obtained, a number of options are available for graphical presen-

tation. Examples of each are given in the next section. First, a profile along one horizontal row of the distorted output waveform can be observed directly for qualitative purposes.

The magnitude of the one-dimensional fast Fourier transform (FFT) of the fringe data can be calculated also, and the strengths of the second and third harmonics measured. The percent harmonic distortion was calculated by the strength of the harmonic, normalized to the strength of the fundamental in that data set. Because broadening of the individual spectral lines is caused by the envelope function $W(x)$ seen in Eq. (1), the strength of any individual harmonic was calculated as the area under the spectrum curve within a small range of frequencies encompassing the 10% response points on each side of the peak.

Another way of presenting the linearity data is also of interest. The input-versus-output curve for the array was obtained by plotting the distorted sinusoidal output values on the vertical axis, while the corresponding irradiance values of the input sinusoid of the same fundamental frequency were plotted on the horizontal axis. When a representative row of data containing many cycles was plotted, a scatter plot representing the responsivity was obtained. Second-degree polynomials were fit to these responsivity curves by a least-squares criterion. This technique directly yields the responsivity and the degree of linearity in graphical form.

For the focal planes tested, the detector-to-detector uniformity was excellent. Thus, a responsivity curve obtained for a single detector was representative of the other detectors in that particular row or of the array as a whole. For a perfectly uniform array of detectors, the interpretation of the spatial-harmonic-distortion test is particularly straightforward, because the input sinusoid provides different detectors with different irradiances rather than characterizing any detector over its entire operating range.

However, the method is still useful in the presence of the detector-to-detector nonuniformity often seen in infrared focal planes.¹⁻³ In Section 5 we present both numerical and analytical models that quantify the relationship between the pixel variance caused by nonuniformity and the minimum detectable harmonic distortion, which determines the ultimate sensitivity of the spatial-harmonic-distortion test.

4. RESULTS

In this section, we compare the responses obtained from the two arrays tested: a vidicon tube camera and a solid-state CID camera. We present linearity data in the following forms: flat-field plots, direct waveforms, responsivity curves, and Fourier spectra. We also present data on the percent harmonic distortion versus spatial frequency for both cameras.

4.1. Flat-field plots

Figures 2(a) and 2(b) show flat-field plots for the CID and the vidicon, respectively. The curves show representative detector output in digital units versus the input irradiance, at zero spatial frequency. The solid-state camera has a higher degree of linearity, as expected.

4.2. Direct waveforms

Figures 3(a) and 3(b) are representative plots of direct array data for the CID and the vidicon, respectively, both at a spatial frequency of 12.5 cycles/cm. The distorted (nonsinusoidal) nature of the waveform output from the vidicon is evident.

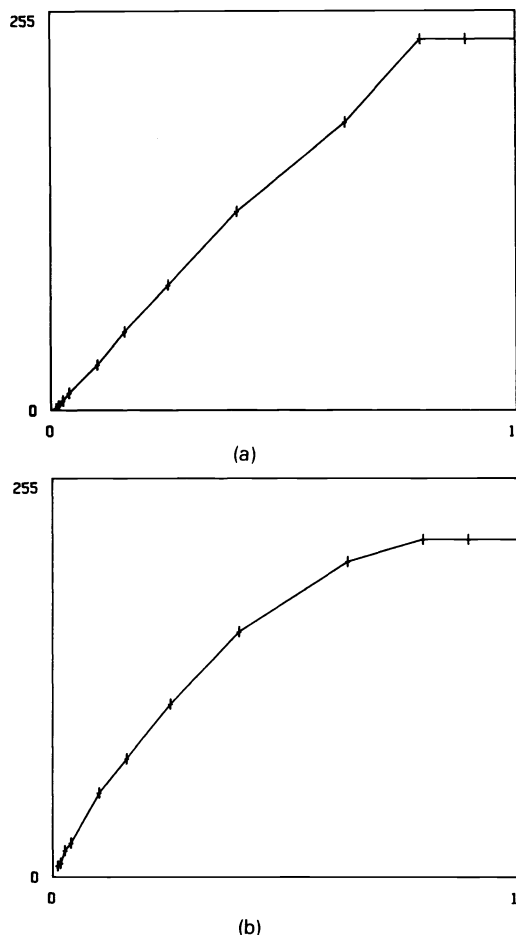


Fig. 2. Measured flat-field curve for the (a) CID array, (b) vidicon. Vertical axis is in A/D converter output units. The horizontal axis is in irradiance units, with 1 unit along the axis equal to $10 \mu\text{W}/\text{cm}^2$.

4.3. Responsivity curves

Figures 4(a) and 4(b) are representative plots of input-versus-output curves, that is, the responsivity functions for the CID and the vidicon. These plots were measured at 25 cycles/cm. As mentioned in Section 3, these curves were made by plotting the distorted sinusoidal output values on the vertical axis, while the corresponding irradiance values of the input sinusoid of the same fundamental frequency were plotted on the horizontal axis. The plotted points are the resulting data over a number of cycles of the waveform, while the solid lines are the least-squares best fit of a second-degree polynomial. Again, the more linear response of the CID camera is evident.

4.4. Spectra

Figures 5(a) and 5(b) show representative plots of the magnitude of the Fourier spectra of array output data at a spatial frequency of 12.5 cycles/cm, for the CID and the vidicon, respectively. The second harmonic is clearly seen for both cameras, even though it is smaller for the CID array, which has a more linear response. The third harmonic is also visible in the vidicon data. The harmonic components to be measured must have sufficient strength with respect to the baseline noise in the spectra. As seen in Section 5, this noise arises because of detector-to-detector nonuniformity, and determines the ultimate sensitivity of the test in terms of the minimum detectable nonlinearity.

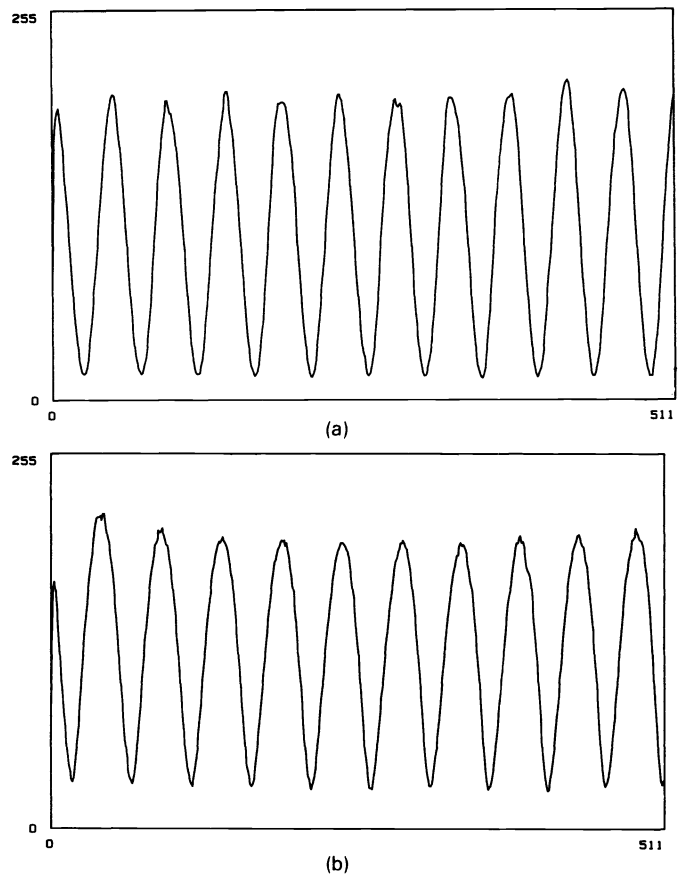


Fig. 3. Representative direct array data, at 12.5 cycles/cm, for the (a) CID array, (b) vidicon. Vertical axis is in A/D converter output units. The horizontal axis is in position units, with 512 units along the axis equal to 1 cm. Note especially the nonsinusoidal nature of the vidicon data.

4.5. Percent harmonic distortion versus spatial frequency

Figures 6(a) and 6(b) show the dependence of second-harmonic distortion on spatial frequency for the CID array and the vidicon, respectively. The harmonic distortion is a decreasing function of spatial frequency for both arrays. This spatial-frequency dependence is a quantity that cannot be measured by the usual flat-field linearity test. Although we do not postulate a mechanism in this article, the interpretation of a spatial-frequency-dependent nonlinearity for detector arrays would be analogous to artifacts such as the adjacency effect seen in photographic media.

5. TEST SENSITIVITY LIMITATION: SPATIAL NONUNIFORMITY

The concept and interpretation of the spatial-harmonic-distortion test are straightforward when all of the detectors have the same responsivity function. This may be very nearly the case for certain focal planes, but for other focal planes an appreciable detector-to-detector nonuniformity exists. Generally, digital correction algorithms yield a decrease in the magnitude of the nonuniformity, but still leave some residual variation due to the limited number of points of correction.¹⁻³

In this section, we present numerical and analytical models for the sensitivity of the spatial-harmonic-distortion test to the presence of pixel-to-pixel nonuniformity.

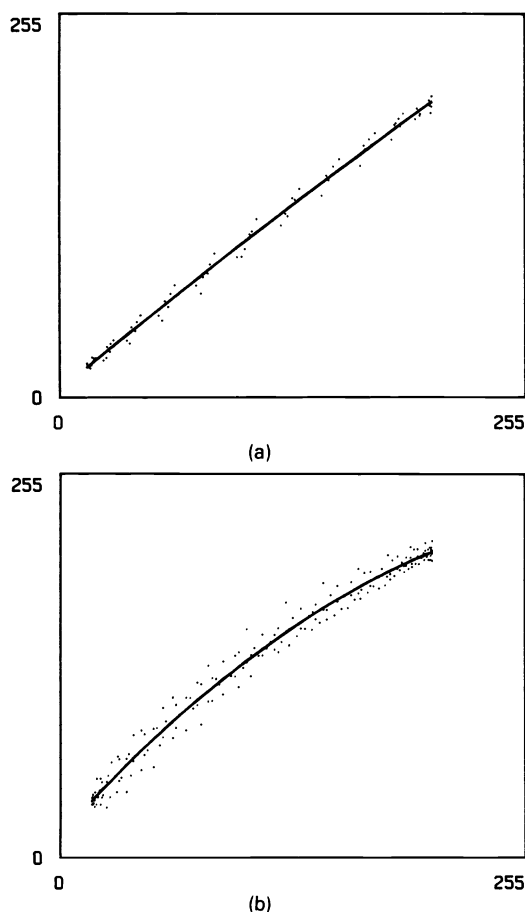


Fig. 4. Responsivity curves for (a) CID and (b) vidicon. Data were taken at a spatial frequency of 25 cycles/cm for each. Vertical axis is in A/D converter output units. The horizontal axis is in irradiance units, with 255 units along the axis equal to $7.5 \mu\text{W}/\text{cm}^2$.

5.1. Numerical model

Our numerical model allows the representation of a typical focal-plane response, assuming that the responsivities of the detectors have been corrected for differences in gain and offset to the accuracy of a two-point correction. This model provides valuable qualitative insight into the origin of spatial noise in the presence of nonlinearity and allows the direct visualization of the effect of residual nonuniformity in the Fourier-transform domain.

A two-point correction for gain and offset is most accurate in the vicinity of a central operating range of irradiance that contains the calibration points used to compute the correction. Outside this central region, the slope of the true responsivity curve will eventually deviate from the slope computed for the two-point correction. Because of pixel-to-pixel nonuniformity, the responsivity outside the central region will not be the same for all detectors in an array, but will exhibit a spatial variation.

Our model assumes that an ideal sinusoid of irradiance is input to an array of detectors that exhibits this type of behavior. We assume a responsivity slope of unity (no distortion) for values of the input sine wave within the interval -0.5 to 0.5 , with a stochastic distribution of slopes outside that interval to account for the spatial nonuniformity. We model the slope outside of the central region as being uniformly distributed between 0 and 0.5 .

The central features of our numerical model are that the nonlinearity is created by the difference in responsivities for different regions of irradiance, and that the spatial nonuniformity is cre-

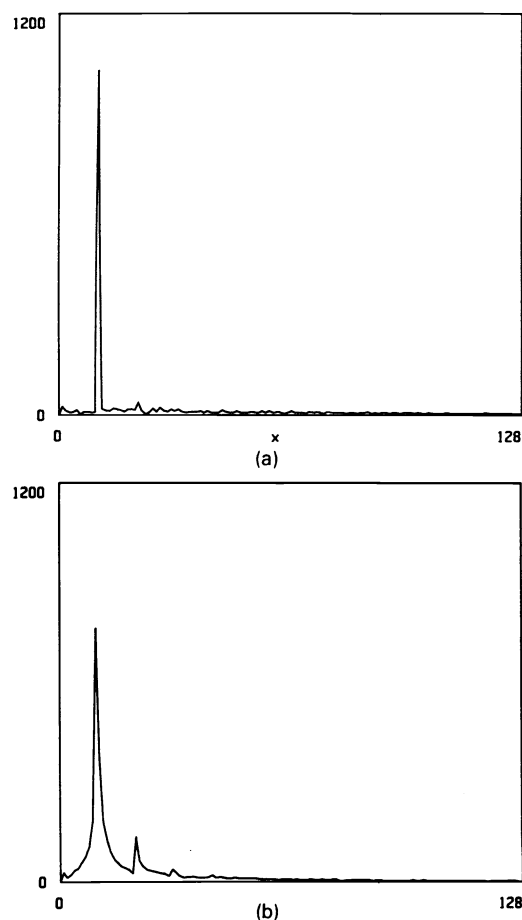


Fig. 5. Magnitude of the Fourier spectrum of the array data for the (a) CID array and (b) vidicon at 12.5 cycles/cm. The vertical axis is the transform magnitude. The horizontal axis is spatial frequency, with 128 units along the axis corresponding to 165 cycles/cm.

ated by the stochastic nature of the slopes of the responsivity curves for irradiances lying outside of the region of best correction.

The random nature of the output waveform, when Fourier-transformed, produces a baseline noise in the spectrum. Figure 7 shows a representative output waveform, and Fig. 8 shows the magnitude of the spectrum for that waveform which results from the model. The second and third harmonics are still clearly discernible, but indeed there is some competition from the baseline noise. The relationship between residual nonuniformity and the minimum detectable harmonic distortion is quantified in the following analytical model.

5.2. Analytical model

To obtain a quantitative relationship between the amount of pixel-to-pixel nonuniformity and the minimum detectable nonlinearity, we take the simple model of a spatially varying signal (either sinusoidal or distorted), which is immersed in zero-mean Gaussian-distributed white noise, of standard deviation σ . Let the fractional amount of nonuniformity present (\mathcal{N}) be defined as the ratio of σ to the maximum output range (\mathcal{R}) of the array:

$$\mathcal{N} \equiv \sigma/\mathcal{R} \quad (2)$$

If we consider a sinusoidal signal waveform of spatial frequency ξ_0 and with an amplitude that occupies the full range of outputs, we have for the waveform itself

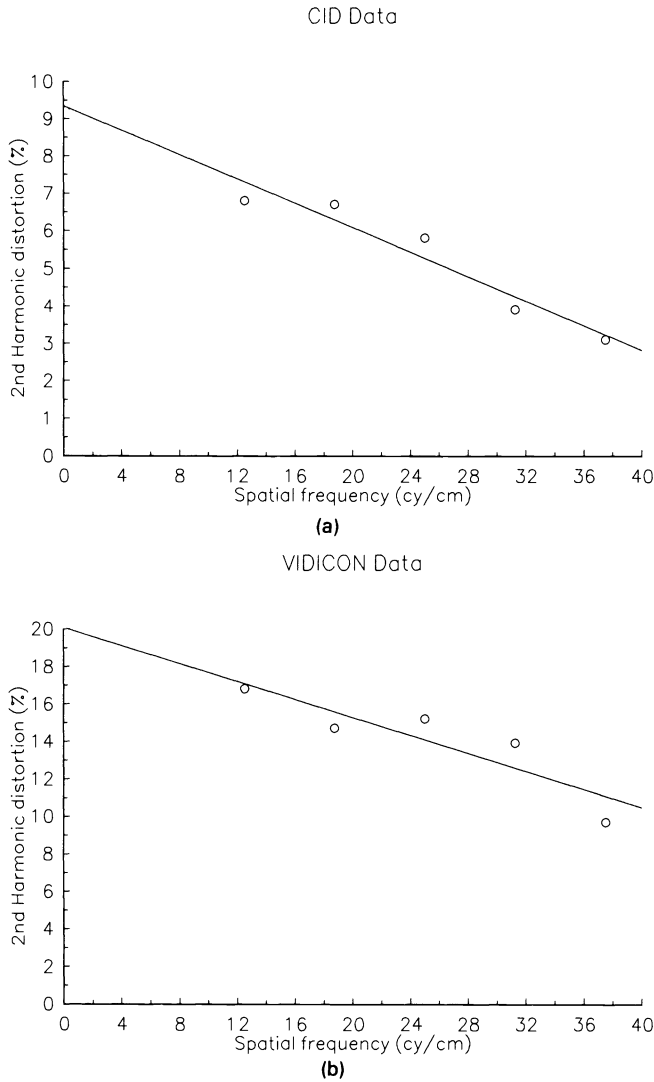


Fig. 6. Second harmonic distortion in percent versus spatial frequency of input sine wave for the (a) CID array, (b) vidicon. The data points shown are for spatial frequencies of 12.5, 18.75, 25, 31.25, 37.5 cycles/cm. The solid line is the best-fit linear curve for each case.

$$s(x) = \frac{\mathcal{R}}{2} \cos(\xi_0 x) . \quad (3)$$

By our definition of the harmonic-distortion magnitude used in Section 3, a second-harmonic component with fractional strength \mathcal{H} will have the following waveform component:

$$h(x) = \mathcal{H} \frac{\mathcal{R}}{2} \cos(2\xi_0 x) . \quad (4)$$

To investigate the visibility of a given amount of harmonic distortion in the presence of nonuniformity, we compare the power spectra of the nonuniformity and the harmonic distortion. The nonuniformity component is properly described by its autocorrelation function $R(x)$, which for the white noise assumed in this section is written as⁸

$$R(x) = \sigma^2 \delta(x) , \quad (5)$$

where δ is the delta function. The Fourier transform of this

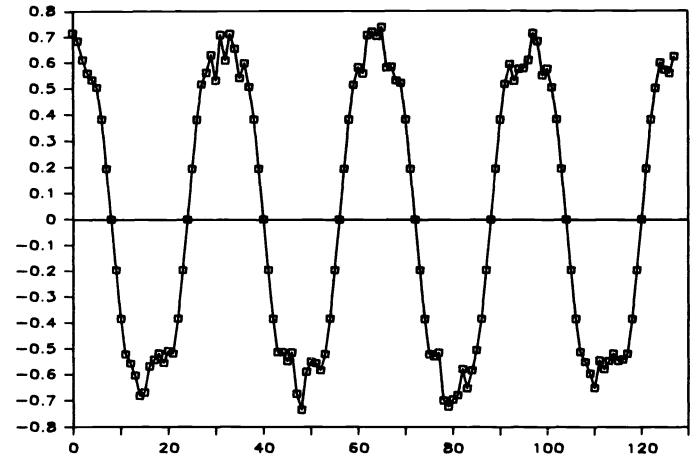


Fig. 7. Numerical model of a distorted output waveform, with a stochastic distribution of responsivities in the detector elements. The vertical axis corresponds to detector output (arbitrary units). The horizontal axis corresponds to position on the array. The array used in the model had 128 elements in the horizontal direction.

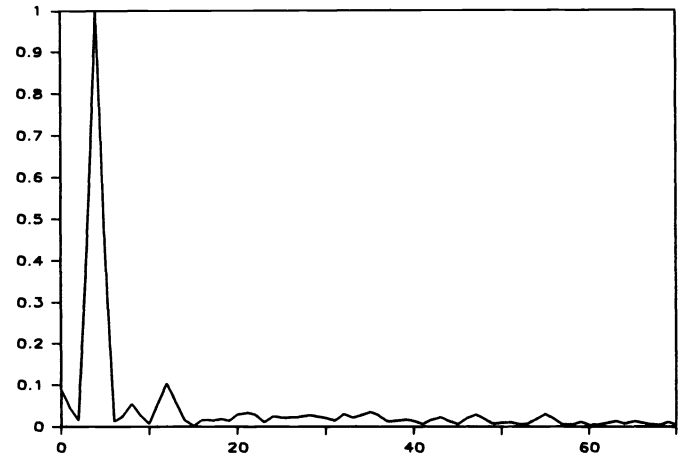


Fig. 8. Magnitude of the Fourier spectrum of the waveform seen in Fig. 7. Horizontal axis corresponds to spatial frequency (arbitrary units). The random distribution of responsivities has contributed to a baseline noise level in the transform, but the second and third harmonics are still discernible.

autocorrelation yields the power spectrum $\text{PSD}(\xi)$ that is a constant function of frequency:

$$\text{PSD}(\xi) = \sigma^2 = (\mathcal{N}\mathcal{R})^2 . \quad (6)$$

The Fourier transform $H(\xi)$ of the harmonic-distortion component $h(x)$ yields

$$\begin{aligned} H(\xi) &= \mathcal{F} \left\{ \mathcal{H} \frac{\mathcal{R}}{2} \cos(2\xi_0 x) \right\} \\ &= \mathcal{H} \frac{\mathcal{R}}{2} \times \frac{1}{2} [\delta(\xi - 2\xi_0) + \delta(\xi + 2\xi_0)] . \end{aligned} \quad (7)$$

The power spectrum, $|H(\xi)|^2$, thus consists of two delta functions of strength $[\mathcal{H}\mathcal{R}/4]^2$. Equating the expressions for $|H(\xi)|^2$ and $\text{PSD}(\xi)$, we obtain the condition for detectability of the harmonic component at a signal-to-noise ratio of unity:

$$[\mathcal{H}\mathcal{R}/4]^2 = (\mathcal{N}\mathcal{R})^2 . \quad (8)$$

Thus, the nonuniformity must be corrected to a level that is one quarter of the harmonic-distortion component to be detected. Thus, for any given focal plane to be tested, the amount of pixel-to-pixel nonuniformity in responsivity will establish the minimum detectable nonlinearity. For example, a system that operated at a full 8-bit dynamic range would allow one level out of 256 for spatial noise, or a nonuniformity of $\approx 0.4\%$. Harmonic distortion could be measured to a level of $\approx 1.6\%$. In a 7-bit system, the minimum detectable harmonic distortion would be in the range of 3%. Nonlinearities of this magnitude would be inconveniently small to observe directly from responsivity curves.

6. CONCLUSIONS

The spatial-harmonic-distortion test is a means for characterization of the nonlinearity in focal-plane arrays. The main advantages of this test, as compared to the usual flat-field method, are the ability to cover the entire operating range of irradiance with one frame of data, the inherent sensitivity of the test to small amounts of nonlinearity, and the ability to measure the spatial-frequency dependence of the nonlinearity. The sensitivity of the test is limited by the (postcorrection) nonuniformity of response from detector to detector, and is in the range of a few percent for systems operating with a 7- to 8-bit dynamic range.

The method should be equally suitable for characterization of visible and infrared focal planes.

7. ACKNOWLEDGMENT

This work was supported under contract DAAL03-86-D-001 by the U.S. Army Night Vision and Electro-Optics Center, Ft. Belvoir, Virginia.

8. REFERENCES

1. C. L. Carrison and N. A. Foss, "Fixed pattern noise compensation techniques for staring infrared focal planes," *Opt. Eng.* 19(5), 753-757 (1980).
2. A. F. Milton, F. R. Barone, and M. R. Krueger, "Influence of nonuniformity on infrared focal plane array performance," *Opt. Eng.* 24(5), 855-862 (1985).
3. G. D. Boreman and C. Costanzo, "Compensation for gain nonuniformity and nonlinearity in HgCdTe infrared charge-coupled-device focal planes," *Opt. Eng.* 26(10), 981-984 (1987).

4. A. B. Carlson, *Communication Systems*, pp. 145-147, McGraw-Hill, New York (1975).
5. T. H. James, ed., *The Theory of the Photographic Process*, Ch. 21, Macmillan, New York (1977).
6. J. M. Stone, *Radiation and Optics*, p. 174, McGraw-Hill, New York (1963).
7. E. O. Brigham, *The Fast Fourier Transform and Its Applications*, pp. 178-188, Prentice Hall, Englewood Cliffs, NJ (1988).
8. H. L. Van Trees, *Detection, Estimation and Modulation Theory*, pp. 197-198, Wiley, New York (1968).



and is a past president of the Florida section of OSA.

Glenn D. Boreman received the BS degree in optics from the University of Rochester in 1978 and the Ph.D. degree in optical sciences from the University of Arizona in 1984. He has held visiting technical staff positions at ITT, Texas Instruments, U.S. Army Night Vision Laboratory, and McDonnell Douglas. Dr. Boreman has been at the University of Central Florida since 1984 and is currently an associate professor of electrical engineering. He is a member of OSA, IEEE, SPIE, and SPSE



Anthony B. James received the BS degree in electrical engineering from Pratt Institute in New York in 1984 and the MS degree in electrical engineering from the University of Central Florida in 1989. He has held technical staff positions at Garland Instruments and at ACE, Inc., both of Dallas, Texas. He is a member of Tau Beta Pi.

Christopher R. Costanzo received the BS degree in optics from the University of Rochester in 1983 and the MS degree in computer science at George Washington University in 1991. Since 1983 he has been a member of the technical staff with the U.S. Army Night Vision Laboratory, working as an optical engineer. Mr. Costanzo's research interests include infrared CCD arrays, image processing, and artificial intelligence. He is a member of SPIE.